Geoderma 376 (2020) 114562

Contents lists available at ScienceDirect

Geoderma

journal homepage: www.elsevier.com/locate/geoderma

# Predicting soil texture from smartphone-captured digital images and an application

R.K. Swetha[a], Prajwal Bende[b], Kabeer Singh[b], Srikanth Gorthi[a], Asim Biswas[c], Bin Li[d], David C. Weindorf[e], Somsubhra Chakraborty[a,*]

[a] Agricultural and Food Engineering Department, IIT Kharagpur, 721302, India
[b] Electrical Engineering Department, IIT Kharagpur, 721302, India
[c] School of Environmental Sciences, University of Guelph, 50 Stone Road East, Guelph, Ontario N1G 2W1, Canada
[d] Louisiana State University, Baton Rouge, LA, USA
[e] Department of Earth and Atmospheric Sciences, Central Michigan University, Mount Pleasant, MI, USA

ARTICLE INFO

Handling Editor: Budiman Minasny

*Keywords:*
Soil texture
Smartphone
Mobile application
Random forest
Convolutional neural network

ABSTRACT

The rapid and non-invasive prediction of soil sand, silt, and clay is becoming increasingly attractive given the laborious nature of traditional soil textural analysis. This study proposed a novel and cheap setup comprising a smartphone, a custom-made dark chamber, and a smartphone application for predicting soil texture of the dried, ground, and sieved samples. The image acquisition system was used to capture triplicate images from 90 mineral soil samples, representing a wide textural variability from sand to clay. Local features, color features, and texture features were extracted from the cropped images and subsequently used in different combinations to predict laboratory-measured clay, silt, and sand via random forest (RF) and convolutional neural network (CNN) algorithms. Results indicated high prediction accuracy for clay ($R^2$ = 0.97–0.98) and sand ($R^2$ = 0.96–0.98) and moderate prediction accuracy for silt ($R^2$ = 0.62–0.75) using both algorithms. Color features outperformed all other image-extracted features and showed the maximum influence on RF model performance. The better performance of the color features can be attributed to the color features of mineral matter and soil organic matter (SOM). An Android-based smartphone application based on the calibrated CNN model was able to predict and return soil textural values. These results exhibited the potential of the proposed system as a proximal sensor for rapid, cost-effective, and eco-friendly soil textural analysis using computer-vision and deep learning. More research is warranted to augment the setup design, develop a standalone mobile application, and measure the impacts of soil moisture and high SOM on the model prediction performance to extend the approach for on-site prediction of soil texture.

## 1. Introduction

Modern innovations in precision agricultural techniques and sensors have resulted in profitable agricultural enterprises (Higgins et al., 2019). Advanced technologies have helped to gain accurate information on the soil microclimate while a wide range of studies has already established the suitability of on-the-go soil sensors (Kheiralla et al., 2016; Ji et al., 2019). The advantages of these sensors come from their ability to offer relatively cheaper high-density measurements. Among soil physical parameters, soil texture is an important attribute that influences several soil properties like water and nutrient holding capacity, density or compaction, air movement, complexation by humus, soil erosion potential, etc. Rapid and cost-effective quantification of soil texture can be an important tool for precision agriculture (Heggemann et al., 2017) and sustainable soil management. Proper knowledge of soil textural variability can be helpful for judicious agronomic practices in diverse crop growth conditions.

In the laboratory, conventional soil textural analysis involves cumbersome processes like drying, grinding, and sieving before time-consuming (~two working days) sedimentation analysis of sand, silt, and clay using hydrometer or pipette (Gee and Bauder, 1986). This approach, while delivers the accurate soil textural results, is not meant for rapid and high-density textural evaluation for spatial variability analysis. Besides, these methods require $H_2O_2$, a corrosive reagent to destroy the native soil organic matter (SOM). Although an advanced laser diffraction particle size analyzer can generate the textural report

* Corresponding author at: Agricultural and Food Engineering Department, Indian Institute of Technology Kharagpur, Kharagpur 721302, India.
*E-mail address:* somsubhra@agfe.iitkgp.ac.in (S. Chakraborty).

https://doi.org/10.1016/j.geoderma.2020.114562
Received 25 April 2020; Received in revised form 23 June 2020; Accepted 27 June 2020
0016-7061/ © 2020 Elsevier B.V. All rights reserved.

with a wide dynamic range and flexibility, this method is also fraught with several limitations like high-cost and sampling errors, particularly with finer fractions (Di Stefano et al., 2010; Fisher et al., 2017). Therefore, there is a need for developing a rapid and sophisticated but cheaper technology for measuring soil texture (Vendrame et al., 2012; Sudarsan et al., 2016, 2018; Qi et al., 2019; Fu et al., 2020).

Recently, several proximal sensors have been successfully utilized for rapid and cost-effective measurement of soil textural parameters. Viscarra Rossel et al. (2007) used a hyperspectral γ-ray spectrometer to predict soil texture. Zhu et al. (2010) used a portable X-ray fluorescence spectrometer (PXRF) to satisfactorily predict the soil texture of 584 soil samples collected from geographically and physiographically diverse regions of North America. Villas-Boas et al. (2016) used laser-induced breakdown spectroscopy (LIBS) for the rapid quantification of soil texture. Moreover, hyperspectral visible near-infrared diffuse reflectance spectroscopy (VisNIR DRS) has become well known for quickly and simultaneously quantifying multiple soil parameters including soil texture by analyzing the soil surface reflected radiation (Hermansen et al., 2017). Generally, VisNIR DRS uses a white light source to illuminate the soil surface and collects reflected energy. The energy is carried into a spectroradiometer via fiber optic cable and parsed at 1–10 nm intervals from 350 to 2500 nm. Following appropriate spectral pre-treatment (e.g., first derivative, standard normal variate, etc.), regression procedures (e.g., random forest, support vector regression, penalized spline regression; partial least squares regression) are used to predict unknowns from a training dataset, in much the same way that unknown pH values are determined after first creating a calibration equation with several known standards. Viscarra Rossel et al. (2006) concluded that mid-infrared DRS (mid-IR DRS) is also adept at predicting soil textural fractions given its sensitivity to quartz and clay. Yet, both VisNIR DRS and mid-IR DRS are non-imaging spectroscopic techniques and require extensive experience in spectral data processing and modeling to deduce meaningful interpretation.

While the rapidity and *in-situ* applicability of PXRF, LIBS, and DRS techniques can be outweighed by their high cost and rare accessibility especially in developing countries where funds are extremely limited for soil characterization, easily accessible devices like the digital camera and smartphone have gained attention in predicting multiple soil parameters. Soil color is a consequence of soil mineral and organic constituents. Scientists have calibrated SOM and soil organic carbon via image-extracted soil color as a proxy (Visacarra Rossel et al., 2008; Fu et al., 2020). Microscopic image analysis has been already used for capturing and describing soil micromorphological features (Sudarsan et al., 2016). With the advancement of digital image processing, computer vision, and deep learning it is now possible to explore soil features in soil section images (Sofou et al., 2005; Marcelino et al., 2007; Elyeznasni et al., 2012). However, preparing soil thin section relies on complex preprocessing steps and thus impossible to implement *in-situ*. To offset this problem, Sudarshan et al. (2018) proposed methodology involving microscopic image acquisition in conjunction with continuous wavelet transform (CWT)-computer vision algorithm to rapidly predict soil texture, both *in-situ* and *ex-situ*. Qi et al. (2019) used microscope-captured soil images to satisfactorily predict soil texture via bag of visual words (BoVW) model and multivariate partial least squares regression (PLSR). Notably, the BoVW algorithm was used to extract soil surface features like color and roughness which were then correlated with sand, silt, and clay via PLSR.

Smartphones are portable, inexpensive, and less subjective in soil color determination than the Munsell color chart. Further, a smartphone with good image acquisition capability can be useful for examining the soil morphology. Aitkenhead et al. (2016) used soil profile images captured via smartphone to predict soil texture. However, they were unable to achieve high prediction accuracy for sand, silt, and clay, possibly due to the heterogeneity of the field conditions. The same group of authors used digital RGB photography in tandem with neural network modeling to predict soil texture but could not achieve good prediction accuracy (Aitkenhead et al., 2018) due to a limited number of input variables. Morais et al. (2019) combined digital image processing and multivariate image analysis to predict soil texture. Despite Gómez-Robledo et al. (2013) have established the potential of smartphone as a reliable soil-color sensor, still, there is a lack of a comprehensive approach where smartphone images can be effectively utilized to generate textural prediction using a smart phone application. Moreover, inconsistency and variability in the image acquisitions systems and the image processing algorithms also limited the applicability and advancement of this research.

Notably, random forest (RF) is a powerful ensemble learning algorithm that uses hundreds of decision trees to predict/classify a sample (Breiman, 2001). In general, each tree is built from a bootstrap sample drawn from the calibration set. At each node of the tree, the candidate set of the predictor is a random subset (mtry) of all the predictors. The final prediction of a new observation is calculated as the average of the predictions from all the trees in the forest. Researchers have established that the RF ensemble shows better prediction than an individual tree. Recently, scientists have used RF for soil type classification via geographic object-based image analysis (Dornik et al., 2018). Chagas et al. (2016) have used RF to spatially predict soil surface texture. Convolutional neural network (CNN) is another powerful algorithm that has been extensively used for image processing and object detection (Cai et al., 2016; Zhang et al., 2016; Vardhana et al., 2018). Notably, CNN is a deep learning method that can differentiate images from each other by allocating learnable weights and biases to several objects in the image. A useful feature of CNN is its capability to detect the spatial and temporal dependencies present in an image.

Therefore, in this research, we aim to develop a novel and inexpensive setup (image acquisition system) comprising a smartphone, a custom-made dark chamber and a smart phone application for predicting soil texture using dried, ground, and sieved samples in laboratory via RF and CNN algorithms. We hypothesize that the soil images acquired via the proposed system will be able to predict soil textural parameters using computer vision, machine learning, and deep learning.

## 2. Materials and methods

### 2.1. Sample description

A total of 90 soil samples were collected randomly in deference to site accessibility, covering three ecoregions of West Bengal province of India including the coastal saline zone (CSZ), alluvial, and lateritic zone, to ensure the variation in soil types. The CSZ soils are naturally formed by the action of tidal water. Contrariwise, reddish Lateritic soils are old soils showing redoximorphic attributes and are characterized by their honeycomb structure. CSZ soil samples represented Akshayanagar (Fine, mixed, hyperthermic, Typic Endoaquepts) and Patibunia (Fine-loamy, mixed, hyperthermic, Typic Endoaquepts) soil series whereas laterite samples represented Teltaka (Fine-loamy, mixed, hyperthermic, Aeric Endoaqualfs) and Ruisanda (Fine, mixed, hyperthermic, Vertic Endoaqualfs) soil series (Nayak et al., 2001; Soil survey staff, 2014). Alluvial soils were collected from Indo-Gangetic alluvial plain and represented Shyampur (Fine, mixed hyperthermic, Aeric Endoaquepts) soil series. Samples were collected from the mineral soil surface (0–15 cm) of fallow croplands using a standard trowel per Schoeneberger et al. (2012), after discarding any vegetation present at the surface. Sample trowel was cleaned between soil collection and sufficient distance between samples (at least 200 m) was maintained to ensure reasonable independence between collected samples. For geolocating and future spatial analysis, the sampling points were uploaded in a Garmin E-trex global positioning system receiver (Garmin, Olathe, KS). Samples were collected in labeled zip-lock bags and transported back to the soil chemistry laboratory of IIT Kharagpur. Before laboratory analyses, all samples were oven-dried (105 °C) and ground to pass

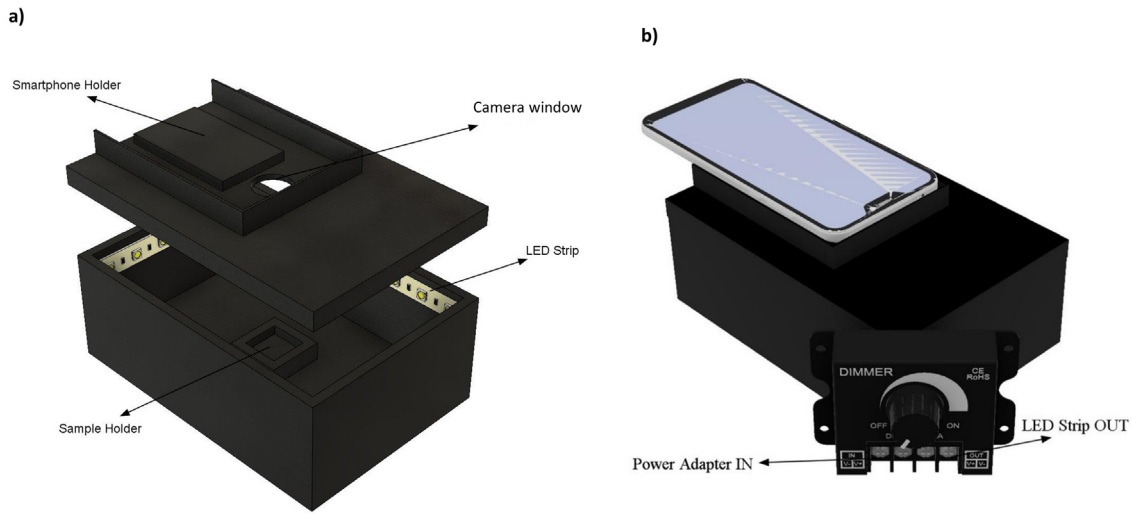


**Fig. 1.** Isometric views of a) the dark chamber interior and b) the complete assembly.

a 2-mm sieve. A modified hydrometer method was used to determine soil texture with clay determinations made at 1440 min with a soil hydrometer (ASTM model 152H) (Gee and Bauder, 1986). Separately, 1 g of air-dried, and ground sample was used to measure SOM by dichromate acid oxidation followed by titration (Nelson and Sommers, 1996).

### 2.2. Setup for image acquisition

A smartphone image capturing dark chamber (12 cm × 8 cm × 5 cm) was constructed using recycled item (a cardboard box), LED strip powered by a DC power adapter, and a LED bulb dimmer switch illumination controller (Fig. 1a and b). The box was entirely painted with black color to avoid any reflection of light within the box. A square-shaped (2 cm × 2 cm × 1 cm) holder was mounted on the bottom part of the box and was used to hold the soil sample. A round window was opened at the top of the box to hold the smart phone camera for capturing images of the soil samples. The white-colored LED strip ran through the vertical faces of the wall whose brightness was controlled using the external dimmer switch. The box was designed to capture images at a fixed distance. To maintain the desired pixel depth, the optimum field of view was observed at a distance of 4.5 cm from the soil surface. Dried and ground soil sample was uniformly packed in the holder using a spatula and a Xiaomi Poco F1 smartphone equipped with a 12.1-megapixel camera was used to capture the images (4032 × 3024 pixels) from 4.5 cm above. The smartphone was kept in a holder designed outside the box for stable support. To achieve consistent image acquisition, the dark chamber was constructed to standardize the image capturing variables like the soil sample and detector positions and illumination. The captured images were saved as a Joint Photographic Experts Group (JPEG) file. For removing the bias, 3 images were taken per sample with three different levels of illumination [high (~600 l×), medium (~500 l×), and low (~400 l×)] using the dimmer. A total of 270 images were generated from 90 samples for subsequent image processing and prediction.

### 2.3. Image processing and soil texture modeling

All image analyses were performed in Python 3.6 environment (Python Software Foundation, DE, USA). the first step of image processing involved selection of the region of interest (ROI). The ROI was selected for a square-shaped area of 1800 × 1800 pixels with 96 dpi of horizontal and vertical resolution and 24 dpi bit depth from the center of the image and used for subsequent feature extraction and representation. All 270 images were randomly divided into training (n = 180, ~66%) and testing set (n = 90, ~33%) for executing texture prediction models.

#### 2.3.1. Feature extraction and representation

Fig. 2 represents the methodological flowchart used in the feature space extraction and subsequent modeling. Initially, the bag of visual words (BoVW) model, an algorithm for language processing and information recovery from text documents, was used for image feature extraction and feature representation. The conventional scale-invariant feature transform (SIFT)-BoVW algorithm relies on local features or local descriptors extraction, codebook or visual dictionary representation using k-means clustering, local feature quantization into visual words using the codebook, and image representation by visual words. For more details on BoVW, see Qi et al, (2019).

The nature of soil images is frequently characterized by various colors and textures of its diverse local components. While the use of soil texture and color has been already established for soil image classification, the shape of soil particles and contours was not that effective due to the inherent variability of soil appearance. Since the traditional SIFT-BoVW model does not utilize any color and texture information in the image description, it may affect soil classification performance. Therefore, we incorporated soil color histogram values and texture information with the SIFT key points, generating a more robust color-texture-SIFT-BoVW feature space (hereinafter, referred to as the full feature space).

Color [HSV (hue, saturation, value) color histogram values and Hu moments], and texture [local binary patterns (LBP) and Harallick features] were used as additional features for soil image analysis. For HSV color histogram values, the RGB color space of the cropped images was transformed into HSV components which were then represented by a 512-dimension feature vector. Moreover, the Hu Moments, which is a set of seven numbers computed using central moments that are constant to image transformations, were also computed. The first six moments were invariant to translation, scale, rotation, and reflection while the 7th moment's sign changed for image reflection. Apart from color, the LBP algorithm which is traditionally used for detecting faces in an image was used to calculate certain texture features of the soil image. LBP detects points surrounding a central point and evaluates if the surrounding points are greater than or less than the central point, generating a binary result. Thus, the LBP operator is an excellent measure of the spatial structure of local image texture. For producing the LBP histogram values using the texture, an existing implementation in the 'skimage' package was used, with the number of circularly

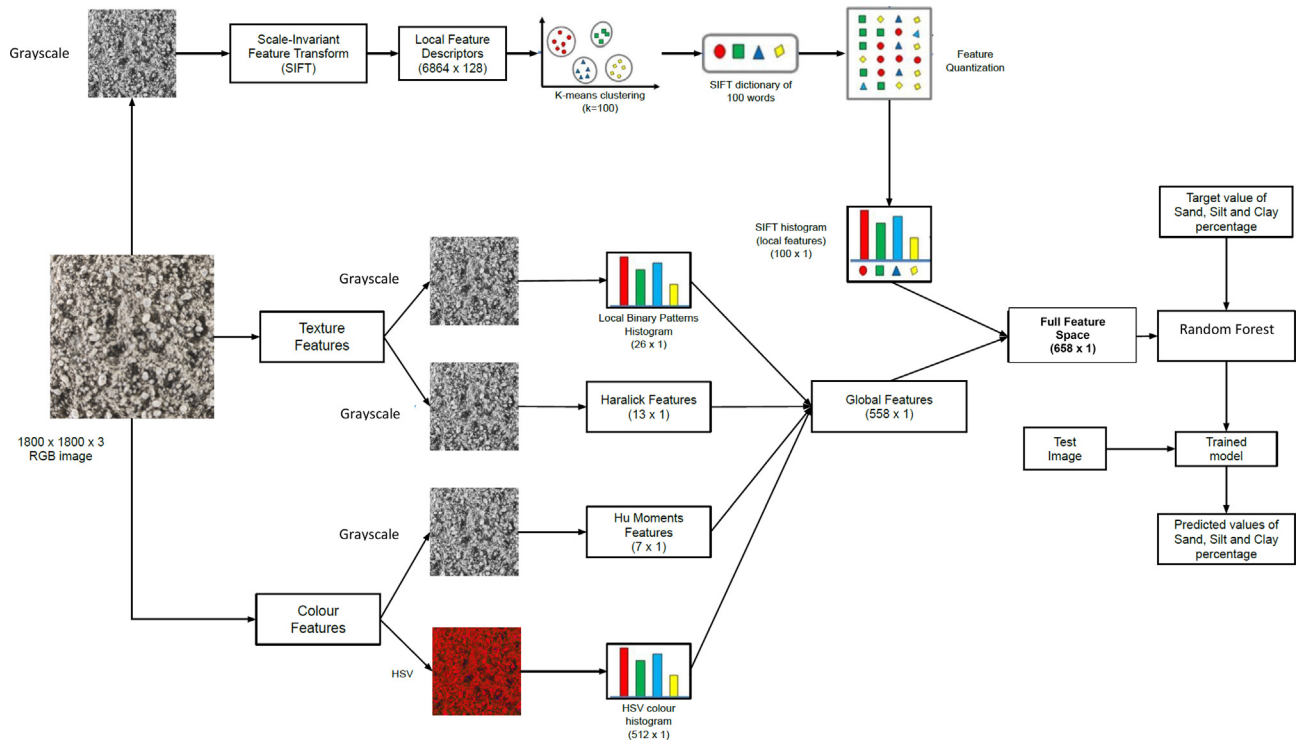


**Fig. 2.** Flowchart showing the scale-invariant feature transform-bag of visual words algorithm, local binary pattern histogram, Haralick features, Hu moments, and HSV color histogram deployed to the smartphone-captured image to represent image features.

symmetric neighbor set points fixed to 24 and the radius of each circle set to 8 pixels, which gave a total of 26 textural features. Also, the Haralick feature algorithm was used to quantify an image based on its texture (Haralick et al., 1973). Haralick features depend on the gray-level co-occurrence matrix (G). Notably, G is a square matrix with dimension equals to the gray levels of an image (Ng). Element [*i*,*j*] of the matrix G is calculated by counting the number of occurrence of a pixel with value *i* surrounding a pixel with value *j* and subsequently dividing G by the total number of such contrasts (Eq. (1)).

$$G=\begin{bmatrix} p(1,1) & p(1,2) & \cdots & p(1,N_g) \\ p(2,1) & p(2,2) & \cdots & p(2,N_g) \\ \vdots & \vdots & \ddots & \vdots \\ p(N_g,1) & p(N_g,2) & \cdots & p(N_g,N_g) \end{bmatrix} \quad (1)$$

In this study, the Haralick feature used four G matrices to compute a total of 13 textural features for generating the subsequent global features. Before SIFT-BoVW, Hu, LBP, and Haralick feature extraction, the cropped RGB image was converted to a grayscale image. The color (519 features) and texture (39 features) cumulatively produced a total of 558 global features which were then combined with the 100 SIFT-BoVW local features, generating a total of 658 features for the full feature space. In this study, the SIFT-BoVW model was executed in the 'OpenCV-python' package. Further, 'skimage' and 'mahotas' packages were used for feature extraction.

### 2.3.2. Machine learning and deep learning

Initially, random forest (RF) regression, which is an ensemble learning technique (Breiman, 2001), was used to predict clay, silt, and sand using the color features, texture features, and SIFT-features in different combinations. In this study, the 'randomforest' package in R version 3.6.2. (R Core Team, 2020) was used to execute the RF model with 500 trees. The training dataset was used to build the model while the test set was used to validate the training model performance.

To estimate the relative variable importance in RF prediction models, an increasingly stringent variable contribution evaluation plan was executed. Initially, RF variable importance plots were created for clay, silt, and sand using the full feature space. Subsequently, to evaluate the impact of SIFT, color (HSV + Hu) and texture (LBP + haralicks) features separately on the full feature space RF model performance, the sum of relative importance for each group of variables were plotted after scaling them to a sum of 100. One of the limitations of the RF algorithm to measure the relative variable importance is that it can only randomly shuffle one variable at a time. Consequently, the RF algorithm codes were modified to randomly shuffle a group of variables at a time so that the decrease in prediction accuracy can be attributed to the overall importance from that group of variables (color, texture, and SIFT). To quantify the decrease of prediction accuracy after permutation, the following metrics were calculated: [($R^2$ without permutation – $R^2$ with permutation)/ $R^2$ without permutation].

Moreover, the convolutional neural network (CNN) algorithm was employed using the 'Keras' and 'Tensorflow' packages in Python to predict soil clay, silt, and sand. In this study, a total of eight convolutional layers were applied to the images followed by a dropout layer to avoid overfitting which was then connected to a fully connected network. The output was a 3-dimensional vector representing the clay, silt, and sand contents. The model prediction performance was evaluated using $R^2$, RMSE, residual prediction deviation (RPD), and RPIQ statistics (Chakraborty et al., 2017). Descriptive statistics were generated using the 'NumPy' and 'pandas' packages.

### 2.4. Mobile application development and testing

An Android-based application, 'SoilAnalyser' was developed using Android Studio 3.6 which is Google's integrated development environment (IDE) software, where the pre-trained CNN model was deployed (Fig. 3). A Flask server developed in Python was hosted on Amazon Web Services (AWS) where the application was used as a client to send images captured by the smartphone. All image processing and subsequent sand, silt, and clay predictions were executed in server and the weights of the trained CNN model were saved during the model

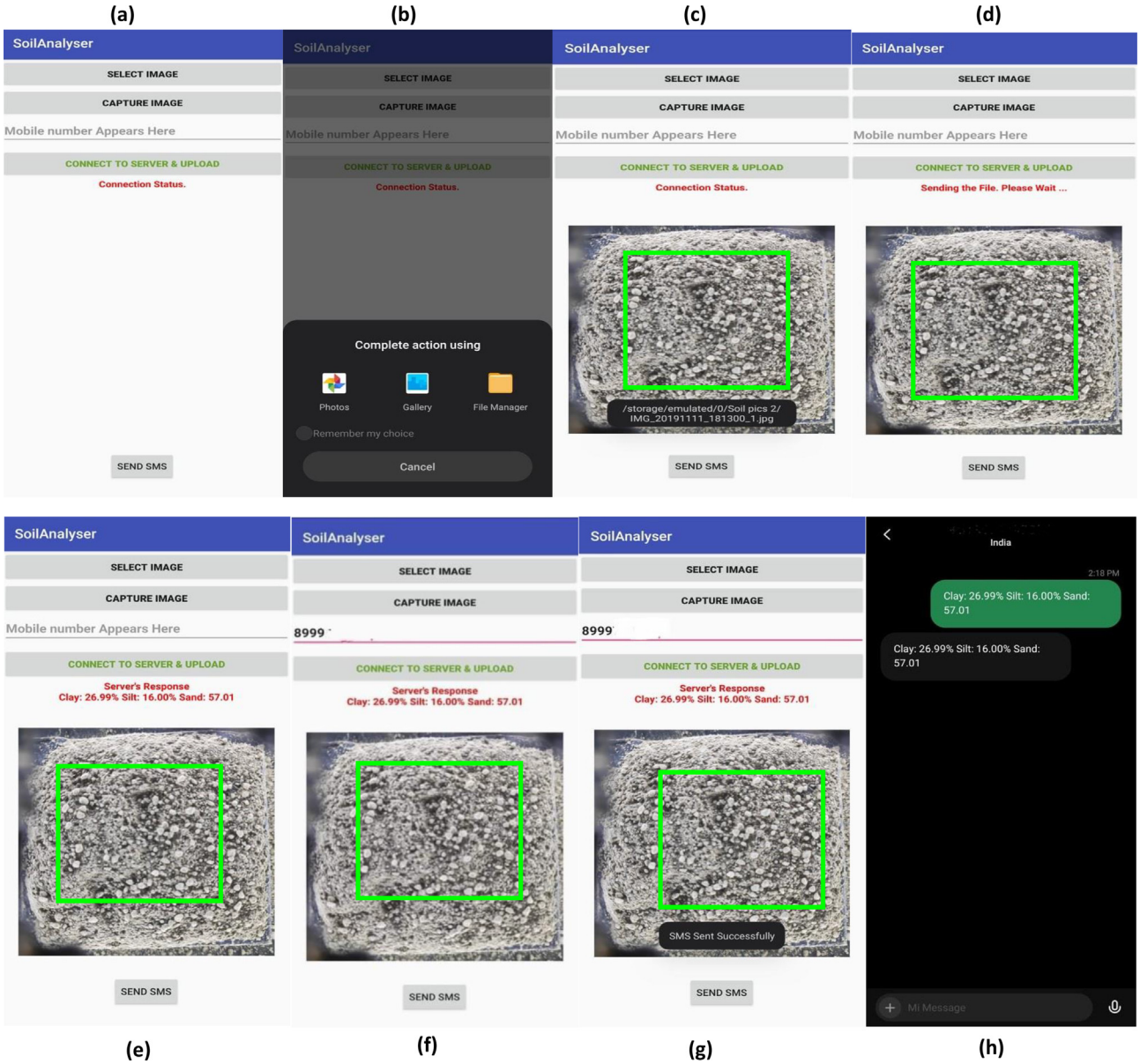


**Fig. 3.** The screen of the smartphone running the SoilAnalyzer Android app for predicting soil texture: a) the main menu; b) and c) image selection; d) uploading the files to the server; e) CNN model predicted soil textural values; f) and g) sending results to the end user via SMS; and h) textural values received at the end user.

training process. The predicted clay, silt, and sand values were then sent to the user through short message service (SMS) which was executed by integrating the SmsManager application program interface (API) in the SoilAnalyzer application. SmsManager accepts mobile number and string variables as arguments. Notably, a user can also query multiple images at a time through this application. For more details, see the Supplementary material (SM).

## 3. Results and discussion

### 3.1. Descriptive statistics and soil textural variations

Descriptive statistics of clay, silt, and sand exhibited high variability with CV ranging between 41% and 67%. (Table 1). Clay content ranged between 4 and 79% with a mean of 32.08%. Sand also exhibited a wide range (13–92%) with an average of ~55% and a standard deviation of 22.62%. Nevertheless, relatively less variability was observed for silt (3–22%), indicating a small range. Clay content exhibited moderate skewness (0.892). All three soil separates exhibited flatter non-normal distribution with negative kurtosis, justifying the use of non-parametric regression like RF and CNN. While the SOM content of the tested mineral soils also exhibited wide variability from 0.20 to 3.63%, it yielded a significant negative correlation with sand ($r = -0.97$) and a significant positive correlation with clay ($r = 0.63$). Conversely, a moderate positive correlation was observed between SOM and silt ($r = 0.53$). According to the USDA textural triangle (Fig. 4), soil samples used in this study were grouped into five textural classes: sand, loamy sand, sandy loam, sandy clay loam, and clay. The cropped smartphone captured images of one representative sample for each textural group are also shown in Fig. 4, exhibiting both visual color and textural variability.

### 3.2. Modeling results and performance of the mobile application

Table 2 summarizes the RF and CNN model validation statistics for predicting clay, silt, and sand. For both clay and sand, RF models using image-derived features in different combinations showed almost similar model generalization capabilities. Besides, for predicting silt, RF models

**Table 1**
Descriptive statistics of clay, silt, sand, and SOM in 90 soil samples used for image analysis and modeling.

| Statistic | Min | Max | 1st Quartile | Median | 3rd Quartile | Mean | Standard deviation | CV (%) | Skewness (Pearson) | Kurtosis (Pearson) |
|---|---|---|---|---|---|---|---|---|---|---|
| Clay (%) | 4 | 79 | 21.25 | 27.00 | 31.00 | 32.08 | 21.53 | 67 | 0.892 | −0.335 |
| Silt (%) | 3 | 22 | 8.00 | 14.00 | 18.00 | 12.95 | 5.71 | 44 | −0.367 | −1.264 |
| Sand (%) | 13 | 92 | 53.00 | 55.00 | 64.75 | 54.95 | 22.62 | 41 | −0.239 | −0.690 |
| SOM (%) | 0.20 | 3.63 | 2.15 | 2.68 | 2.95 | 2.37 | 0.85 | 36 | −1.09 | 0.111 |

using texture, color, and SIFT + color + texture features (full feature space) produced similar validation results. While using the full feature space, clay and sand predicting models produced $R^2$ values of 0.98 and 0.97, respectively, closely following the 1:1 line (Fig. 5). Conversely, model performance worsened while predicting silt ($R^2$ = 0.70, RPD = 1.84). Nonetheless, RF models with color features only (HSV + Hu) were generally very close in performance to the full feature models (Table 2, Fig. 5), and exhibited a close agreement between model-predicted soil separates and laboratory-measured values. Thus, with deference to the law of parsimony, RF predictive models using color features in isolation appeared to be preferable for the prediction of clay, silt, and sand. As indicated in Table 2, the CNN models for all three soil separates produced better results than RF prediction models and thus used for subsequent mobile application development. The better performance of CNN stems from the fact that it can "see" the image at a deeper level as a composition of various edges, lines, corners and capture the contents of the image. The validation RMSE for predicting the clay content varied from 2.77 to 3.48% among all tested models which was encouraging since clay generally shows the highest uncertainty in traditional laboratory textural measurements. This can be attributed to the high resolution of the smartphone camera. Comparing the prediction performance for clay, silt, and sand, approach documented herein produced better results than those reported by Sudarshan et al. (2018) ($R^2$ values of 0.48–0.87 and 0.56–0.88 for coarse fractions and fine fractions, respectively) and Qi et al. (2019) ($R^2$ values of 0.77, 0.68, and 0.71 for sand, silt, and clay, respectively) using microscopic images of air-dried soil samples. The proposed methodology also produced better soil texture prediction than Aitkenhead et al. (2018) ($R^2$ values of 0.25, 0.19, and 0.18 for sand, silt, and clay, respectively) who used digital RGB photos in tandem with the neural

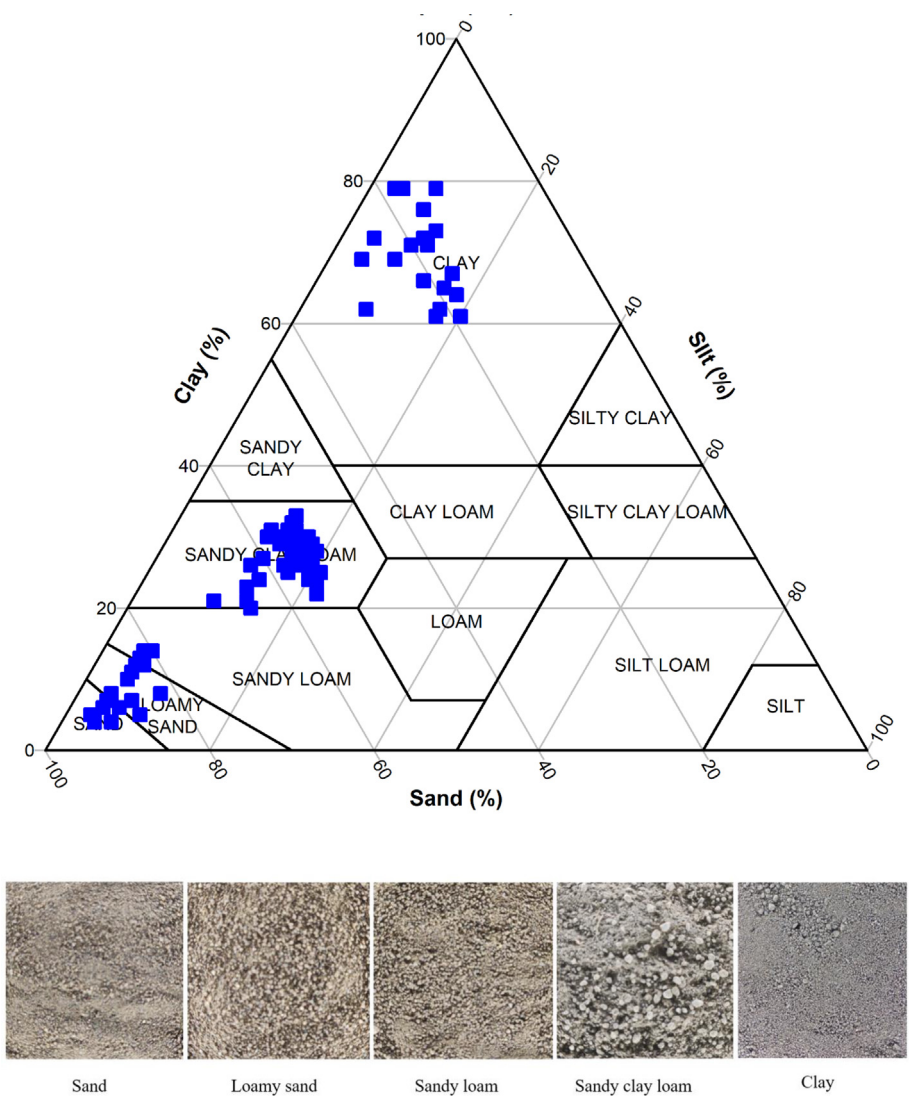


**Fig. 4.** USDA soil texture triangle representing all samples distributed in five textural groups and cropped images of one representative sample from each group.

**Table 2**
Random forest and CNN model validation performance for using image-derived features in different combinations.

| Target | Model | Features | Validation $R^2$ | Validation RMSE (%) | RPD | Bias | RPIQ |
|---|---|---|---|---|---|---|---|
| Clay (%) | RF | SIFT | 0.97 | 3.39 | 6.42 | −1.3 | 3.23 |
| | RF | color | 0.97 | 3.45 | 6.32 | −0.8 | 3.18 |
| | RF | texture | 0.98 | 3.24 | 6.72 | −1.2 | 3.39 |
| | RF | SIFT + color | 0.97 | 3.48 | 6.27 | −0.9 | 3.16 |
| | RF | SIFT + texture | 0.98 | 3.18 | 6.86 | −1.2 | 3.45 |
| | RF | color + texture | 0.98 | 3.41 | 6.38 | −0.9 | 3.21 |
| | RF | SIFT + color + texture[a] | 0.98 | 3.33 | 6.54 | −0.9 | 3.30 |
| | CNN | RGB image | 0.98 | 2.77 | 7.87 | −0.3 | 3.96 |
| Silt (%) | RF | SIFT | 0.62 | 3.60 | 1.63 | 0.2 | 3.32 |
| | RF | color | 0.71 | 3.13 | 1.88 | 0.2 | 3.83 |
| | RF | texture | 0.64 | 3.49 | 1.69 | 0.3 | 3.43 |
| | RF | SIFT + color | 0.69 | 3.25 | 1.81 | 0.2 | 3.69 |
| | RF | SIFT + texture | 0.63 | 3.53 | 1.66 | 0.2 | 3.39 |
| | RF | color + texture | 0.71 | 3.15 | 1.87 | 0.2 | 3.80 |
| | RF | SIFT + color + texture | 0.70 | 3.19 | 1.84 | 0.1 | 3.75 |
| | CNN | RGB image | 0.75 | 2.94 | 2.00 | 0.1 | 4.08 |
| Sand (%) | RF | SIFT | 0.96 | 4.56 | 4.89 | 1.4 | 1.97 |
| | RF | color | 0.97 | 3.82 | 5.83 | 0.8 | 2.35 |
| | RF | texture | 0.96 | 4.59 | 4.85 | 1.3 | 1.95 |
| | RF | SIFT + color | 0.97 | 3.77 | 5.90 | 0.8 | 2.38 |
| | RF | SIFT + texture | 0.96 | 4.28 | 5.19 | 1.4 | 2.09 |
| | RF | color + texture | 0.97 | 3.75 | 5.94 | 0.8 | 2.39 |
| | RF | SIFT + color + texture | 0.97 | 3.87 | 5.76 | 0.9 | 2.32 |
| | CNN | RGB image | 0.98 | 2.90 | 7.70 | 0.2 | 3.11 |

[a] Color-texture-SIFT-BoVW feature space, also known as the full feature space.

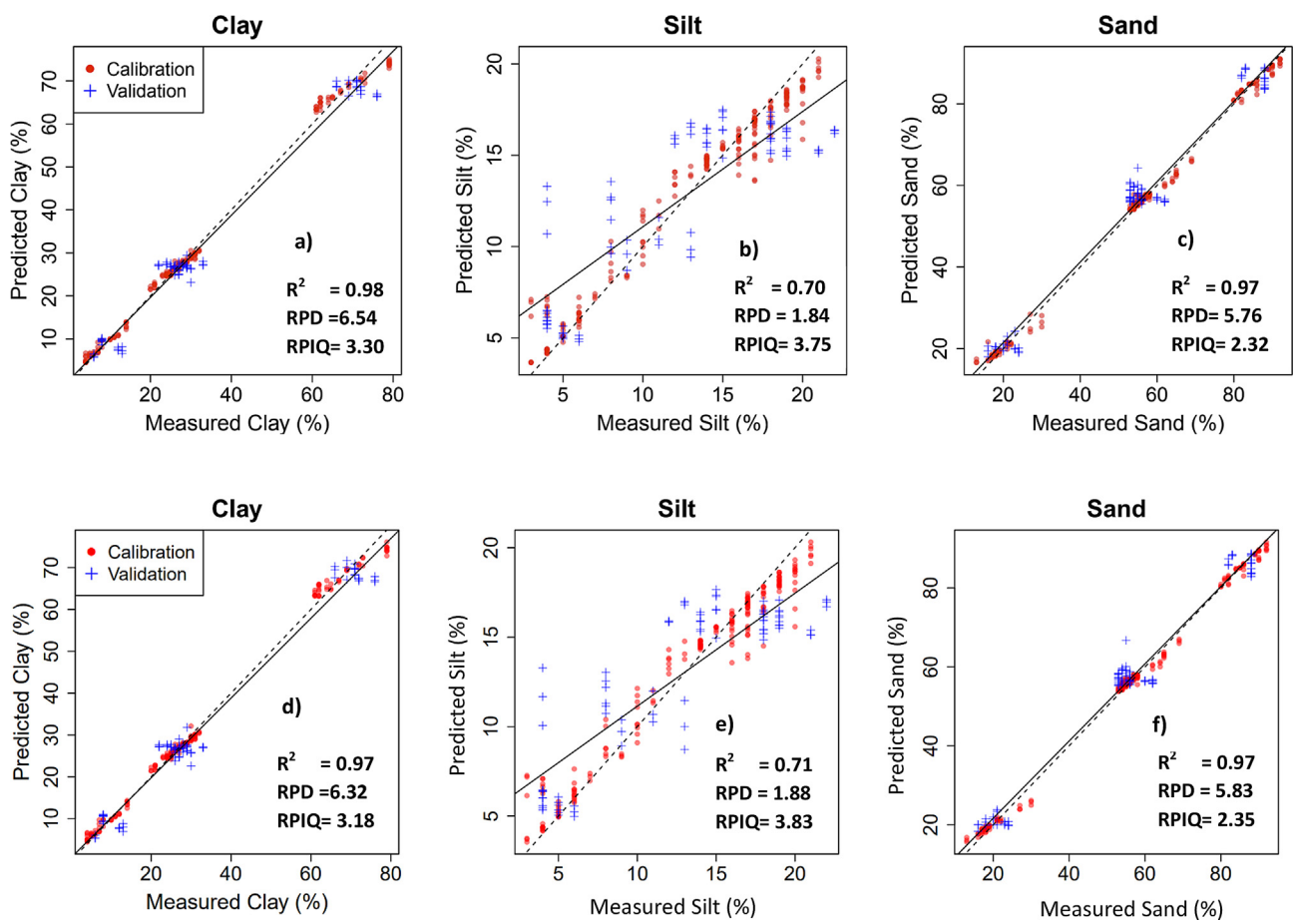


**Fig. 5.** Random forest predicted vs laboratory-measured plots for a) clay using full feature space, b) silt using full feature space, c) sand using full feature space, d) clay using color features only, e) silt using color features only, and f) sand using color features only. The dashed line represents the 1:1 line while the solid line represents the regression line.

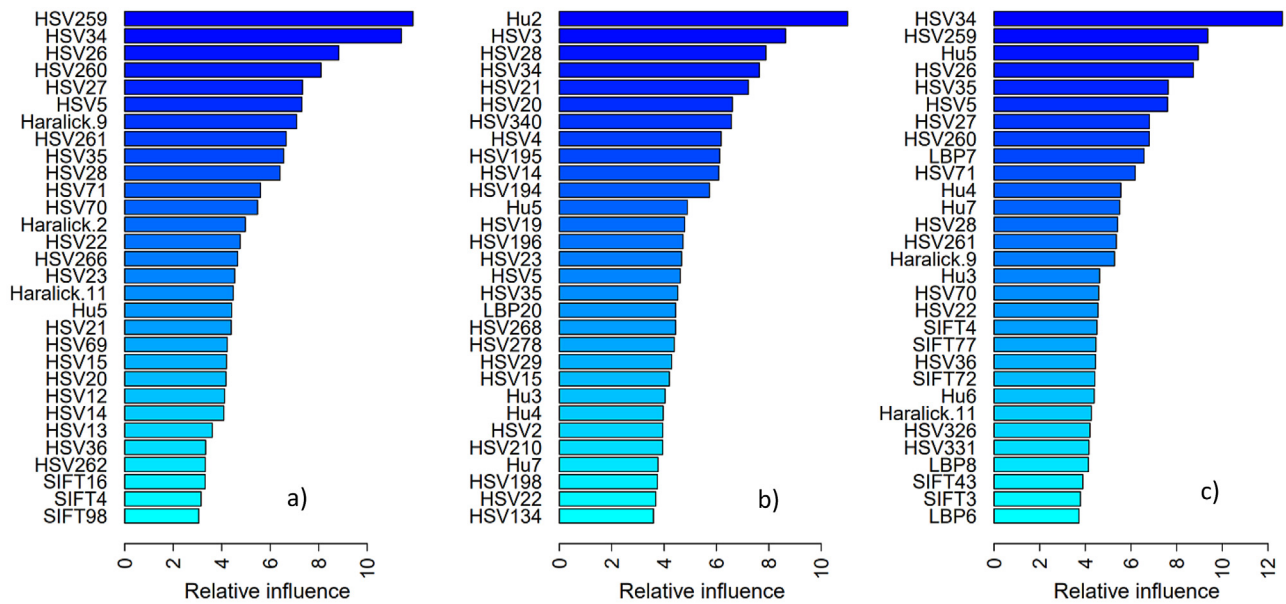


**Fig. 6.** Random forest variable importance plots for a) clay using full feature space, b) silt using full feature space, and c) sand using full feature space.

network model to predict soil texture. Sand prediction by the approach documented herein (RPD values of 4.85–7.70) outperformed DRS-based sand prediction with RPD values below 2 (Viscarra Rossel et al., 2006). This study also produced lower RMSEs for clay and sand than those reported by using Mid-IR (Minasny et al., 2008) (6.31% and 6.23% for sand and clay, respectively).

The judicious selection of input variables is crucial for portable and user-friendly devices since adding too many predictor variables often causes over-simplification of the predictive model (Noori et al., 2010). Initially, the variable importance plots of the full feature space RF models for clay, silt, and sand exhibited 23, 24, and 15 HSV features, respectively, among the top 30 influential features (Fig. 6). Subsequently, while plotting the sum of relative importance for SIFT, color (HSV + Hu), and texture (LBP + haralicks) features separately on the full feature space RF model performance, the following feature importance was observed for all three soil separates: color > SIFT > color + texture (Fig. 7), justifying the RF model results (Table 2). Finally, the combined variable importance plot for all three separates (Fig. 8) also revealed the same trend as overserved earlier (Fig. 7) where color features outperformed SIFT and texture features.

The better performance of color features can be attributed to the color features of mineral matter and SOM. While in the light-textured soils, the HSV parameters predominantly depicted the influence of mineral color given the negative correlation between sand and SOM ($r = -0.97$), the high coefficient of determination observed while predicting clay may be linked with the combined influence of SOM and clay mineral color on the image-extracted HSV values. A similar influence of SOM color in predicting soil texture was reported by Qi et al. (2019). However, color is not exclusively linked to soil texture and caution must be used in applying such an interpretation. Clays are well known to physically protect organic matter from degradation, thus generally supporting higher organic matter content and darkening the soil via melanizaiton (e.g., in mollisols) (Parton et al., 1994; Bockheim and Gennadiyev, 2000). However, dark color can also be observed in certain sands where the mineralogical origin is from dark colored parent material (e.g., basalt, amphibole, etc.) (Schaefer and Mcgarity, 1980). The influence of mineral color on HSV parameters in the present study stems from the fact that sand particles appear brighter under the LED light of the dark chamber, as reported in other studies (Sudarsan et al., 2016). Furthermore, the presence of Fe-oxides manifested brown color in coarse-textured lateritic soils. Commonly, in soil, SOM acts as a binding agent creating micro-aggregates (Sudarsan et al., 2018). Also, while conducting the chemical particle size analysis, sodium hexametaphosphate is added to the suspension to physically disperse soils which cannot be completely obtained via mechanical grinding employed in the proposed approach. Nevertheless, the high prediction accuracy for clay and the close agreement between the 1:1 line and the RF regression line (Fig. 5) are encouraging, implying that the proposed methodology, involving drying, grinding, and computer vision, did not misinterpret these micro-aggregates as coarse soil separates like silt and sand.

### 3.3. Practical considerations and limitations

The proposed image acquisition system in conjunction with computer vision, machine learning, and deep learning exhibited promise for smartphone-based soil texture prediction in the laboratory. However, a few limitations of the study can be listed. Firstly, more research is warranted so that this methodology can be extended for predicting soil texture on-site after excavating the soil from the field with negligible processing, ensuring significant time and cost savings. Notably, the measurement variability which could probably arise due to the varying moisture content and aggregates, found under field-conditions, were eliminated by the drying, grinding, and sieving of the sample. Indeed, soil moisture is one of the major challenges for image-based proximal soil sensing (Sudarsan et al., 2018) which may produce image distortion in soils with high clay content due to their higher water holding capacity (Qi et al., 2019). Nonetheless, further studies are warranted to measure the impact of these variables on the method performance before drawing a strong conclusion. Both RF and CNN algorithms were able to predict sand and clay with greater accuracy, perhaps since all soils used in this study were mineral soils. However, more deviation is expected in soils with high SOM like peat and muck soils (Sudarsan et al., 2018). For example, organic coated sand grains in the surface mineral horizon often produce dark-colored light-textured soils (Lindbo et al., 1998), confounding the color-based prediction of soil texture. While we do not recommend the elimination of classical laboratory-based particle size analysis, the usefulness of making soil texture predictions with significant time and cost savings still signifies substantial progress in smartphone-based soil science applications. For example, in the present study, one student successfully scanned 90 samples in triplicate using a smartphone in just 4 working hours and no consumable

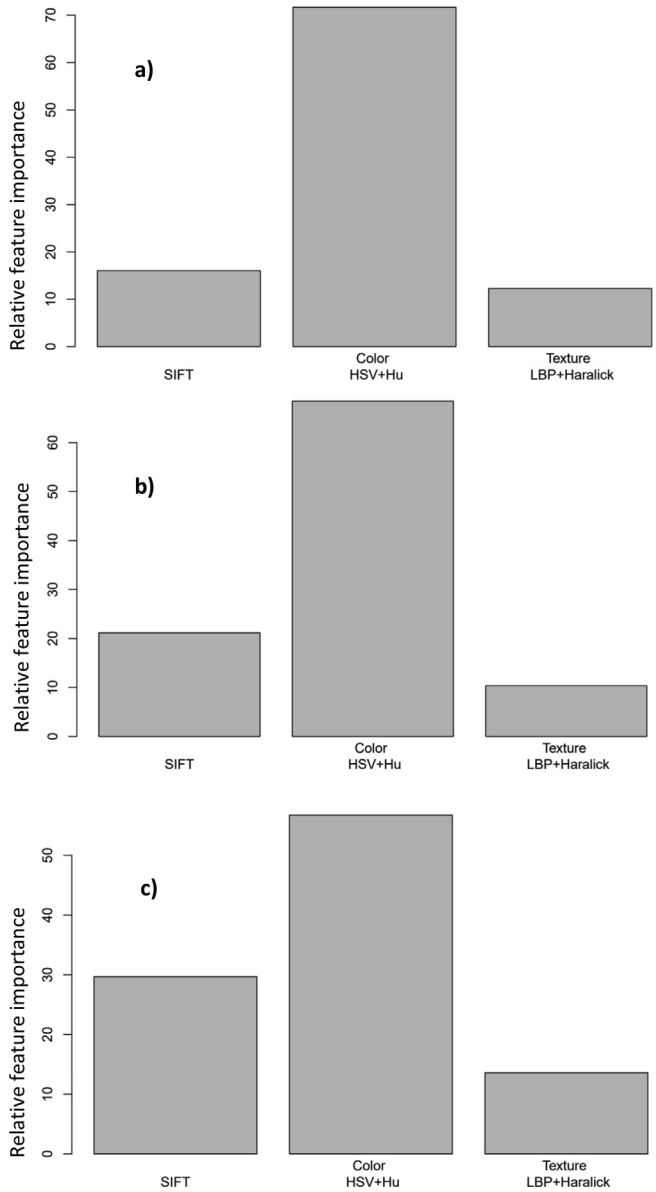


**Fig. 7.** The sum of random forest relative importance for each group of variables used in full feature space models for a) clay, b) silt, and c) sand.

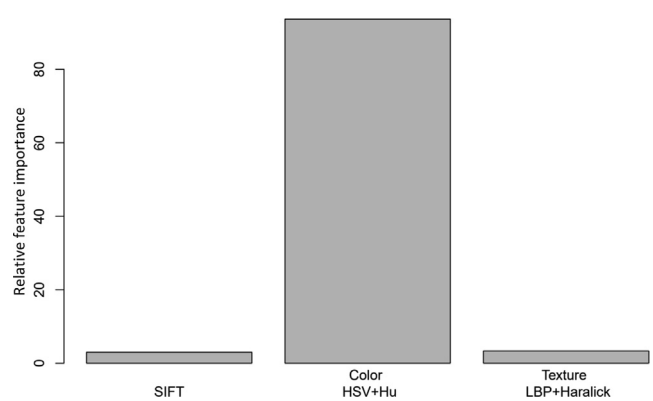


**Fig. 8.** The combined random forest variable importance plot considering all three soil separates.

was purchased. The whole image-acquisition setup costs ~$ 255USD [$ 250 USD for the smartphone + $5 USD for the dark chamber]. The proposed approach could be useful in developing countries where the access to deionized water for particle size analysis and lab space are limited, especially in remote areas. But even in those areas, people now have the access of rudimentary smartphones.

Admittedly, since the majority of soil samples represent only three textural classes (sand, loamy sand, and clay), one should use caution while interpreting the coefficient of determination values of the tested RF and CNN models (Fig. 5, Table 2). Specifically, the absence of samples from all 12 textural classes and the unavailability of enough silty samples somewhat limited the scope and performance of the tested models. While the proposed method offered similar error (< 5%) as compared to the conventional laboratory methods, it is necessary to include more images from a wide range of soil samples to validate the robustness of smartphone-based soil texture analysis. Also, since the RGB values of a similar color show variability due to their device-dependency (Westland and Ripamonti, 2004), a variety of smartphones with the similar resolution tested in this study must be evaluated to validate the methodology reported herein. Also, the developed mobile application needs to be standalone so that it can automatically extract image features and run the model locally inside the same smartphone to produce an objective and accurate textural prediction. Notably, for the successful application of the proposed approach for other areas, soil image libraries need to be representative of the soils of the region of interest which further underscores the importance of robust local calibration models with a large sample number. Consequently, there is a need for worldwide collaboration where soil images collected at multiple laboratories should be used to develop multiple local prediction models.

## 4. Conclusions

This study reports on a novel and cheap setup comprising a smartphone, a custom-made dark chamber and a smart phone application for predicting soil texture using dried, ground, and sieved samples in laboratory. The image acquisition system captured triplicate images from 90 soil samples, representing a wide textural variability from sand to clay. Local features (SIFT-BoVW), color features (HSV + Hu), and texture features (LBP + Haralicks) were extracted from the cropped images and subsequently used in different combinations to predict laboratory-measured clay, silt, and sand values via RF and CNN algorithms. Results indicated high prediction accuracy for clay and sand, with moderate prediction accuracy for silt. Among all image-extracted features, color features showed the maximum influence on the model performance. An Android-based application based on the calibrated CNN model was developed. This clearly exhibited the potential of the proposed system for rapid and cost-effective soil textural analysis. More research is warranted to measure the impacts of soil moisture and high SOM on the model prediction performance to extend the approach for predicting soil texture on-site.

## Declaration of Competing Interest

The authors declare that they have no known competing financial interests or personal relationships that could have appeared to influence the work reported in this paper.

## Acknowledgements

The authors wish to thankfully acknowledge financial assistance from the Ministry of Human Resource Development, Govt. of India. The authors gratefully acknowledge the BL Allen Endowment in Pedology at Texas Tech University in conducting this research.

## Appendix A. Supplementary data

Supplementary data to this article can be found online at https://doi.org/10.1016/j.geoderma.2020.114562.

## References


Aitkenhead, M., Cameron, C., Choisy, B., Coull, M., Black, H., 2018. Digital RGB photography and visible-range spectroscopy for soil composition analysis. Geoderma 313, 265–275.

Aitkenhead, M., Coull, M., Gwatkin, R., Donnelly, D., 2016. Automated soil physical parameter assessment using smartphone and digital camera imagery. J. Imag. 2 (4), 35. https://doi.org/10.3390/jimaging2040035.

Bockheim, J.G., Gennadiyev, A.N., 2000. The role of soil-forming processes in the definition of taxa in Soil Taxonomy and the World Soil Reference Base. Geoderma 95 (1–2), 53–72.

Breiman, L., 2001. Random forests. Machine Learning 45, 5–32.

Cai, Z., Fan, Q., Feris, R.S., Vasconcelos, N., 2016. In: A Unified Multi-scAle Deep ConvolutionAl NeurAl Network for FAst Object Detection. Springer, pp. 354–370.

Chagas, C.D.S., Junior, W.D.C., Bhering, S.B., Filho, B.C., 2016. Spatial prediction of soil surface texture in a semiarid region using random forest and multiple linear regressions. Catena 139, 232–240.

Chakraborty, S., Weindorf, D.C., Deb, S., Li, B., Paul, S., Choudhury, A., Ray, D.P., 2017. Rapid assessment of regional soil arsenic pollution risk via diffuse reflectance spectroscopy. Geoderma 289, 72–81.

Di Stefano, C., Ferro, V., Mirabile, S., 2010. Comparison between grain-size analyses using laser diffraction and sedimentation methods. Biosyst. Eng. 106 (2), 205–215.

Dornik, A., Drăguţ, L., Urdea, P., 2018. Classification of soil types using geographic object based image analysis and randomForest. Pedosphere 28 (6), 913–925.

Elyeznasni, N., Sellami, F., Pot, V., Benoit, P., Vieublé-Gonod, L., Young, I., Peth, S., 2012. Exploration of soil microtomography to identify coarse sized OM assemblages. Geoderma 179–180, 38–45.

Fisher, P., Aumann, C., Chia, K., O'Halloran, N., Chandra, S., 2017. Adequacy of laser diffraction for soil particle size analysis. PLoS ONE 12 (5), e0176510.

Fu, Y., Taneja, P., Lin, S., Ji, W., Adamchuk, V., Daggupati, P., Biswas, A., 2020. Predicting soil organic matter from cellular phone images under varying soil moisture. Geoderma 361, 114020.

Gee, G.W., Bauder, J.W., 1986. Particle-size analysis. In: Klute, A. (Ed.), Methods of Soil Analysis. Part 1 — Physical and Mineralogical Methods, second ed. SSSA, Madison, WI, pp. 383–411.

Gomez-Robledo, L., Lopez-Ruiz, N., Melgosa, M., Palma, A.J., Capitan-Vallvey, L.F., Sanchez-Maranon, M., 2013. Using the mobile phone as Munsell soil-colour sensor: an experiment under controlled illumination conditions. Comput. Electron. Agric. 99, 200–208.

Haralick, R., Shanmugan, K., Dinstein, I., 1973. Textural features for image classification. IEEE Trans. Syst. Man Cybern. 3, 610–621.

Hermansen, C., Knadel, M., Moldrup, P., Greve, M.H., Karup, D., de Jonge, L.W., 2017. Complete soil texture is accurately predicted by visible near-infrared spectroscopy. Soil Sci. Soc. Am. J. 81 (4), 758–769.

Heggemann, T., Welp, G., Amelung, W., Angst, G., Franz, S.O., Koszinski, S., Schmidt, K., Pätzold, S., 2017. Proximal gamma-ray spectrometry for site-independent in situ prediction of soil texture on ten heterogeneous fields in Germany using support vector machines. Soil Tillage Res. 168, 99–109.

Higgins, S., Schellberg, J., Bailey, J.S., 2019. Improving productivity and increasing the efficiency of soil nutrient management on grassland farms in the UK and Ireland using precision agriculture technology. Eur. J. Agron. 106, 67–74.

Ji, W., Adamchuk, V.I., Chen, S., Mat Su, A.S., Ismail, A., Gan, Q., Shi, Z., Biswas, A., 2019. Simultaneous measurement of multiple soil properties through proximal sensor data fusion: a case study. Geoderma 341, 111–128.

Kheiralla, A.F., El-Fatih, W.T., Abdellatief, M.K., El-Talib, Z.M., 2016. Design and development of on-the-go SoilpH mapping system for precision agriculture. In: *In:* Proceedings of the 2016 IEEE Conference of Basic Sciences and Engineering Studies (SGCAC), IEEE, pp. 192–195.

Lindbo, D.L., Rabenhorst, M.C., Rhoton, F.E., 1998. Soil colour,organic carbon, and hydromorphy relationships in sandy epipe-dons. Quantifying Soil Hydromorphology. SSSA Special Pub-lication No. 54. Soil Science Society of America, Madison, WI,USA, pp. 95–105.

Marcelino, V., Cnudde, V., Vansteelandt, S., Caro, F., 2007. An evaluation of 2D-image analysis techniques for measuring soil microporosity. Eur. J. Soil Sci. 58 (1), 133–140.

Minasny, B., McBratney, A.B., Tranter, G., Murphy, B.W., 2008. Using soil knowledge for the evaluation of mid-infrared diffuse reflectance spectroscopy for predicting soil physical and mechanical properties. Eur. J. Soil Sci. 59 (5), 960–971.

Morais, P.A.O., de Souza, D.M., Carvalho, M.T.M., Madari, B.E., de Oliveira, A.E., 2019. Predicting soil texture using image analysis. Microchem. J. 146, 455–463.

Nayak, D.C., Sarkar, D., Velayutham, M., 2001. Soil series of West Bengal. Publication No. 89. Nagpur: National Bureau of Soil Survey and Land Use Planning.

Nelson, D.W., and L.E. Sommers. 1996. Total carbon, organic carbon and organic matter. In: Sparks, D.L. (Ed.), Methods of soil Analysis: Chemical methods, Part 3. Soil Science Society of America, Madison, WI. pp. 961–1010.

Noori, R., Karbassi, A., Sabahi, M.S., 2010. Evaluation of PCA and Gamma test techniques on ANN operation for weekly solid waste prediction. J. Environ. Manage. 91 (3), 767–771.

Parton, W.J., Ojima, D.S., Cole, C.V., Schimel, D.S., 1994. A general model for soil organic matter dynamics: Sensitivity to litter chemistry, texture, and management. In: Bryant, R.B., Arnold, R.W. (eds.) Quantitative modeling of soil forming processes. Soil Science Society of America Special Publication 39. Madison, WI.

Qi, L., Adamchuk, V., Huang, H., Leclerc, M., Jiang, Y., Biswas, A., 2019. Proximal sensing of soil particle sizes using a microscope-based sensor and bag of visual words model. Geoderma 351, 144–152.

R Core Team, 2020. R: A language and environment for statistical computing. R Foundation for Statistical Computing, Vienna, Austria. Available online at: http://www.Rproject.org (Verified on 29 March 2010).

Schaefer, B.M., Mcgarity, J.W., 1980. Genesis of red and dark brown soils on basaltic parent materials near Armidale, N.S.W., Australia. Geoderma 23 (1), 31–47.

Schoeneberger, P.J., Wysocki, D.A., Benham, E.C., 2012. Field book for describing and sampling soils. Version 3.0. USDA-NRCS, National Soil Survey Center, Nebraska.

Sofou, A., Evangelopoulos, G., Maragos, P., 2005. Soil image segmentation and texture analysis: a computer vision approach. IEEE Geosci. Remote Sens. Lett. 2 (4), 394–398.

Soil Survey Staff, 2014. Keys to soil taxonomy. In: USDA-Natural Resources Conservation Service, 12th ed. U.S. Government Print Office, Washington, D.C., USA.

Sudarsan, B., Ji, W., Biswas, A., Adamchuk, V., 2016. Microscope-based computer vision to characterize soil texture and soil organic matter. Biosyst. Eng. 152 (1), 41–50.

Sudarsan, B., Ji, W., Adamchuk, V., Biswas, A., 2018. Characterizing soil particle sizes using wavelet analysis of microscope images. Comput. Electron. Agric. 148, 217–225.

Vardhana, M., Arunkumar, N., Abdulhay, E., 2018. Convolutional neural network for biomedical image segmentation with hardware acceleration. Cognit. Syst. Res. 50, 10–14.

Vendrame, P.R.S., Marchão, R.L., Brunet, D., Becquer, T., 2012. The potential of NIR spectroscopy to predict soil texture and mineralogy in Cerrado Latosols. Eur. J. Soil Sci. 63 (5), 743–753.

Villas-Boas, P.R., Romano, R.A., de Menezes Franco, M.A., Ferreira, E.C., Ferreira, E.J., Crestana, S., Milori, Bastos Pereira, D.M.,, 2016. Laser-induced breakdown spectroscopy to determine soil texture: a fast analytical technique. Geoderma 263, 195–202.

Visacarra Rossel, R.A., Fouad, Y., Walter, C., 2008. Using a digital camera to measure soil organic carbon and iron contents. Biosyst. Eng. 100, 149–159.

Viscarra Rossel, R.A., Taylor, H.J., McBratney, A.B., 2007. Multivariate calibration of hyperspectral γ-ray energy spectra for proximal soil sensing. Eur. J. Soil Sci. 58 (1), 343–353.

Viscarra Rossel, R.A., Walvoort, D.J.J., McBratney, A.B., Janik, L.J., Skjemstad, J.O., 2006. Visible, near infrared, mid infrared or combined diffuse reflectance spectroscopy for simultaneous assessment of various soil properties. Geoderma 131, 59–75.

Westland, S., Ripamonti, C., 2004. Computational colour science using Matlab, 1st ed. Wiley, New York.

Zhang, L., Yang, F., Zhang, Y. D., Zhu, Y. J., 2016. Road crack detection using deep convolutional neural network. In: Proceedings of 2016 IEEE International Conference on Image Processing; 2016 Sep 25–28; Phoenix, AZ, USA. Piscataway: IEEE; 2016. pp. 3708–12.

Zhu, Y., Weindorf, D.C., Chakraborty, S., Haggard, B., Johnson, S., Bakr, N., 2010. Characterizing surface soil water with field portable diffuse reflectance spectroscopy. J. Hydrol. 391, 133–140.